3-D Interconnected Magnetic Nanofiber Networks With Multifunctional Properties

Tristan da Câmara Santa Clara Gomes[1], Joaquín De La Torre Medina[2], Yenni G. Velázquez-Galván[1], Juan M. Martínez-Huerta[3], Armando Encinas[3], and Luc Piraux[1]

[1]Institute of Condensed Matter and Nanosciences, Université Catholique de Louvain, B-1348 Louvain-la-Neuve, Belgium
[2]Instituto de Investigaciones en Materiales—Unidad Morelia, Universidad Nacional Autónoma de México, Morelia 58190, Mexico
[3]División de Materiales Avanzados, Instituto Potosino de Investigación Científica y Tecnológica, San Luis Potosí 78216, Mexico

3-D alloyed and multilayered interconnected nanofiber networks have been fabricated by electrodeposition techniques, allowing a controlled composition and 3-D structural topology. These features have been found crucial to tailor their magnetic and magneto-transport properties. Their interplay along with the use of a simple analytical model based on the particular interconnected topology of the networks has allowed to accurately determine the anisotropic magnetoresistance (AMR) ratio. The as-obtained AMR ratio for interconnected nanofiber networks is consistent with an average that results from all the nanowires orientations in the membrane. The careful choice of magnetic and non-magnetic layer thicknesses has been decisive for the fabrication of Co/Cu multilayered interconnected nanofiber networks with giant magnetoresistive response as high as 19%. Interconnected nanofiber networks with controlled material composition and specific structural features are very attractive for the development of mechanically stable superstructures suitable for potential technological device applications.

Index Terms—**3-D interconnected nanofiber network, magnetic anisotropy, magnetic multilayers, magnetoresistance.**

I. Introduction

3-D NANOWIRE or nanofiber networks are very appealing nanoarchitectures with controlled topologies and tunable physicochemical properties, which are of particular interest for the development of novel and functional devices. Besides the broad range of applications in solar cells [1], energy harvesting/storage systems [2], and electronic sensing devices and actuators [3], interconnected nanofiber networks are also widely studied because of their interesting magnetic and magneto-transport properties for the development of next-generation multifunctional devices with controlled magnetic anisotropy and microwave absorption properties [4] and for the storage and logic operation of information carried and processed by domain walls flowing along them [5]. Porous polymer membranes with crossed nanochannels have been revealed suitable as templates for the synthesis of 3-D interconnected magnetic nanofiber networks that present interesting magnetic and magneto-transport properties [4], [6], [7]. In this paper, alloyed and multilayered interconnected nanofiber networks have been fabricated with controlled compositions that are easily obtained through careful control of electrodeposition conditions like the deposition potential and using different electrolytic solutions. The interplay between their magnetic and magnetoresistive properties with their composition is found to be crucial to adjust their magnetic and magneto-transport properties. Particularly, increasing the Co content in NiCo alloyed interconnected nanofiber networks leads to the appearance of a magnetocrystalline (MC) anisotropy contribution that decreases the effective out-of-plane magnetization easy axis observed in Ni-rich alloys. A maximum anisotropic magnetoresistance (AMR) ratio is observed for an alloy composition containing 75% of Ni, which increases up to a value of 8% as the temperature decreases down to 20 K. Using a simple analytical model based on the particular interconnected topology of the networks, the AMR ratio has been precisely determined from simple magneto-transport measurements along a single probe direction. The measured AMR ratio for interconnected nanofiber networks is consistent with an average that results from all the nanowire orientations in the membrane. Besides, the observed significant giant magnetoresistive responses in Co/Cu multilayered interconnected nanofiber networks with specific magnetic and non-magnetic layer thicknesses make them interesting systems for potential technological applications. Finally, the above features make these materials very attractive for the development of mechanically stable superstructures suitable for potential technological applications in magnetic memory, sensor, and logic devices.

II. Nanofiber Networks Topology and Fabrication

For the fabrication of interconnected nanofiber network films, 22 μm thick crossed nanoporous polycarbonate (PC) templates have been used, which are prepared by performing a sequential two-step exposure of energetic heavy ions, at various angles in the range from $-45°$ to $+45°$ with respect to the normal of the PC film surface [6]. To this end, a PC film was subjected to a first irradiation step followed by a second irradiation step after rotating the film in the plane by 90° and re-exposed to the same angular variable irradiation flux to form

Manuscript received March 10, 2017; revised June 14, 2017; accepted June 18, 2017. Date of publication June 26, 2017; date of current version October 24, 2017. Corresponding author: L. Piraux (e-mail: luc.piraux@uclouvain.be).

Color versions of one or more of the figures in this paper are available online at http://ieeexplore.ieee.org.

Digital Object Identifier 10.1109/TMAG.2017.2719658

finally a complex 3-D nanochannel network. The latent tracks were chemically etched in a 0.5 M NaOH aqueous solution at 70 °C to form 40 nm diameter nanopores, so the resulting as-prepared polymer membranes have a volumetric porosity of about 20% [4]. The successive track-etching process allows controlling aspects of the template topology, such as the angle between the nanochannels and the template normal, the volumetric porosity, and the mean pore diameter that can be tuned between a few tens of nanometers to a few hundreds of nanometers. In the second stage, the PC templates were coated on one side using an e-beam evaporator with a metallic Cr(10 nm)/Cu(150 nm) bilayer. The template is partially filled from the previously sputtered metallic cathode by an electrode position process allowing the control of the material composition and nano-structuration, such as nanowires, nanotubes, core-shell nanocables, and multilayered nanowires. Interconnected nanofiber networks were grown by electrodeposition into crossed nanoporous PC templates at room temperature in the potentiostatic mode using a Ag/AgCl reference electrode and a Pt counter electrode. Electrodeposition of Ni, NiFe, and Co interconnected nanofiber networks was carried out at the respective constant potentials of -1.1, -1, and -0.95 V using the electrolytes: 1M $NiSO_4{\cdot}6H_2O$ + 0.5M H_3BO_3 at pH 3.4; 20mM $FeSO_4{\cdot}5H_2O$ + 0.5M $NiSO_4{\cdot}6H_2O$ + 0.5M H_3BO_3 at pH 3; and 0.85M $CoSO_4{\cdot}7H_2O$ + 0.5M H_3BO_3 at pH 5.0. The as-prepared solutions have a pH value of 3.6, which was decreased gradually down to 3.0 by addition of diluted H_2SO_4 in the case of NiFe or increased up to 5.0 by addition of NaOH in the case of Co [8]. In the case of the Ni_xCo_{1-x} ($20\% \leq x \leq 75\%$) alloyed interconnected nanofiber networks, electrodeposition was carried out at potentials in the range from -0.85 to -2 V using the electrolyte 1.87M $Ni(SO_3NH_2)_2{\cdot}4H_2O$ + 0.4M $CoSO_4{\cdot}7H_2O$ + 0.5M H_3BO_3. For alloys with $60\% \leq x \leq 90\%$, electrodeposition was done for deposition potentials from -1 to -2 V using the same electrolyte but with a Co concentration of 0.1M $CoSO_4{\cdot}7H_2O$ instead. The pH of the as-prepared NiCo solution was lowered down to 2.2 by addition of H_2SO_4. The multilayered crossed nanowires (CNWs) have been grown from a single sulfate bath using potentiostatic control and a pulsed electrodeposition technique [9]. The composition of the electrolyte was 0.85M $CoSO_4{\cdot}7H_2O$ + 3mM $CuSO_4{\cdot}5H_2O$ + 0.5M H_3BO_3 and the deposition potential was alternatively switched between -0.95 V to deposit Co-rich layers containing approximately 10% Cu impurity, and -0.5 V to deposit almost pure Cu layers [10]. Following a procedure described elsewhere [9], the deposition rates of each metals were determined from the pore filling time. According to this calibration, the deposition time was adjusted to 300 ms and 16 s for the Co and Cu layers, respectively, and the estimated average thickness of the Co and Cu layers was 10 nm.

The morphology of the nanostructured interconnected nanofiber networks was characterized using a field-emission scanning electron microscope (SEM). For the electron microscopy analysis, it was necessary to remove the PC template. This was done by first etching the cathode using a I2:KI (0.1:0.6 M) solution and then dissolving the PC with dichloromethane. Magnetization hysteresis loops were obtained at room temperature in the out-of-plane (OOP) direction of the interconnected nanofiber network film, using an alternating gradient field magnetometer (AGFM-Lakeshore) with a maximum applied field of ±14 kOe. A 500 μm wide and 500 nm thick microstrip line waveguide was evaporated on the free surface of the PC membrane after electrodeposition, which has been used for the ferromagnetic resonance (FMR) measurements as shown schematically in Fig. 1(c) [4], [6]. Room temperature FMR measurements were performed in the field sweep mode in the OOP direction from 10 kOe down to zero field, at a constant frequency in the range of 100 MHz to 50 GHz. The magneto-transport measurements were performed at 20, 150, and 290K while sweeping a magnetic field between ±10 kOe in the in-plane [IP or the y-axis in Fig. 1(d)] and OOP [or the z-axis in Fig. 1(d)] directions. Magneto-transport measurements can be easily performed on interconnected nanofiber network films, with the flow of current restricted along the nanowire segments. For each sample, the input power was kept below 0.1 μW to avoid self-heating, and the resistance was measured within its ohmic resistance range with a resolution of one part in 10^5. For these measurements, the cathode is locally removed to create a two-probe design suitable for easy electric measurements, as shown in Fig. 1(d).

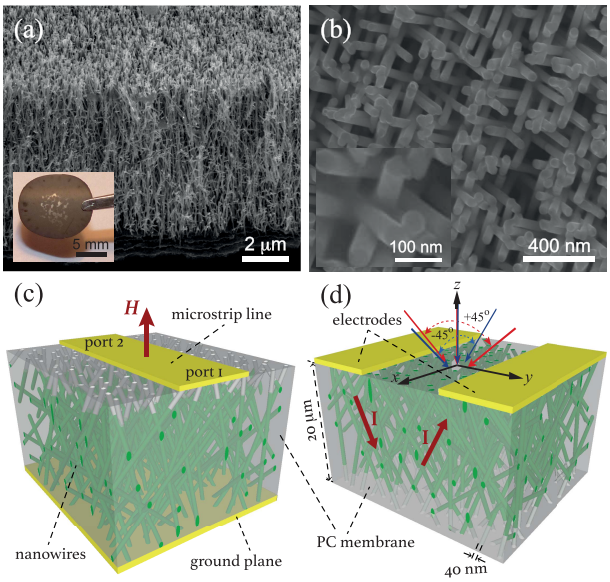

Fig. 1. (a) and (b) SEM images of an interconnected network of electrodeposited 3-D Ni interconnected nanofiber networks, with a NW diameter of 40 nm, obtained after complete dissolution of the host template. The inset in (a) shows a typical size of fabricated devices and their mechanical robustness. (c) Schematic representation of the system after the local removing of the cathode used for electrodeposition leading to a suitable design for two-probe electrical measurement [6], [7]. (d) Schematic of a microstrip transmission line for FMR measurement fabricated using a similar partially filled membrane.

III. Results and Discussion

As shown in Fig. 1(a), interconnected nanofiber network films are mechanically stable and self-supported after dissolution of the porous template. The close views in Fig. 1(b) show

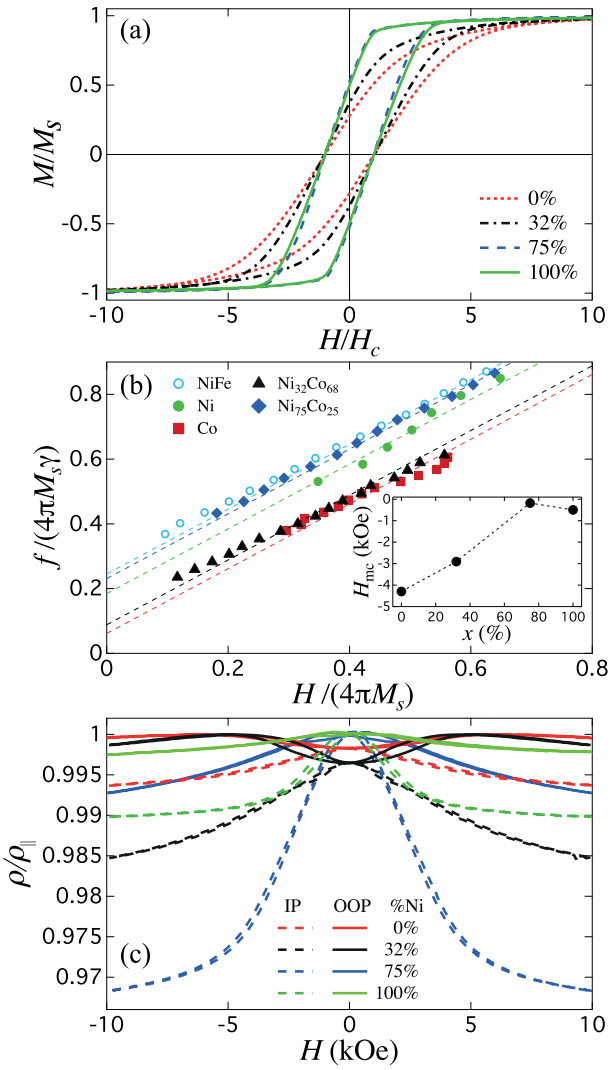

Fig. 2. (a) Normalized hysteresis loops measured with the external field applied in the OOP direction of the PC membrane in Ni_xCo_{1-x} interconnected nanofiber networks, with $0 \leq x \leq 1$. (b) Dependence between the $f/(4\pi M_s\gamma)$ and $H/(4\pi M_s)$ ratios for the samples in (a), along with their corresponding normalized FMR dispersion relations (dotted lines) by the effective field $4\pi M_s$ for an infinite film. The inset shows the variation of H_{mc} as a function of the Ni content. (c) Magnetoresistance curves performed on the same set of samples of (a), with the applied field in the OOP (continuous lines) and IP (dashed lines) directions. All measurements were carried out at room temperature.

overall interconnected topology of the networks, as well as the low roughness of the nanowires. A close relation between the interconnected nanofiber networks' magnetic and structural properties has been demonstrated in NiCo interconnected nanofiber networks, where the magnetic anisotropy can be accurately controlled by changing the alloy composition [7]. The magnetic properties of the interconnected nanofiber networks can be modified by increasing the Ni content, along with a progressive disappearance of the transverse MC anisotropy contribution, which competes with the magnetostatic (MS) anisotropy of the nanowires.

As seen in Fig. 2(a), Ni-rich samples (with $x>45\%$) display fair square hysteresis loops in contrast to the case of the Co-rich samples. Decreasing the Ni content below 45% leads to the appearance of the hexagonal close-packed (HCP) MC anisotropy contribution, which competes with the MS anisotropy contribution since the c-axis is perpendicular to the nanowires axis [7]. Therefore, the magnetic anisotropy of Ni-rich networks is higher than that of Co-rich ones, as expected.

To further investigate the magnetic behavior of the NiCo alloys, FMR measurements have been carried out for the distinct alloyed networks. The effect of the Ni content on the magnetic anisotropy of NiCo networks is clearly observed from their corresponding normalized dispersion relations shown in Fig. 2(b). For pure Co CNW networks, the observed behavior in these figures is very similar to what is reported previously for Co parallel nanowire arrays [8]. That is, the corresponding resonance frequencies are lowered from the pure MS case of a NiFe network [6], which is consistent with the configuration where the c-axis is oriented perpendicular to the nanowire axis in Co-rich networks. These results are in good agreement with what is observed from the hysteresis loops in Fig. 2(a).

The MC contribution for the distinct networks can be obtained using the previously reported expression between the effective field H_{eff} and the zero-field resonance frequency f_0, given by

$$H_{\text{eff}} = \frac{f_0}{\gamma\sqrt{C_2}} \tag{1}$$

where the geometric factor $C_2 = 0.57$ for a maximum angle $\theta = \pi/4$ of the nanowires orientation, as reported previously [6]. The effective field can be written as the superposition of the MS and MC contributions, that is $H_{\text{eff}} = H_{\text{ms}} + H_{\text{mc}}$. The H_{ms} field must be known in order to determine the H_{mc} field. As known, the H_{ms} field can be written as the product of its saturation magnetization (M_s) and a demagnetizing factor (N), which is a key feature of the particular interconnected topology and a common parameter for all the networks. For the particular case of interconnected nanofiber networks with only MS contribution, its effective anisotropy field is equal to the product of M_s and N. Since the N factor remains unknown, let us consider a MS factor N_{M} that is proportional to N, which we define as the ratio between the $H_{\text{ms}} = H_{\text{eff}}$ field in (1) and the MS field ($4\pi M_s$) for an infinite film. Indeed, the factor N_{M} is independent on M_s as it reproduces only the topological features of purely MS interconnected nanofiber networks, which writes

$$N_{\text{M}} = \frac{f_{\text{NiFe}}}{\sqrt{C_2}}. \tag{2}$$

In this equation, $f_{\text{NiFe}} = f_0/(4\pi M_s\gamma)$ is the normalized zero-field resonance frequency for the NiFe network shown in Fig. 2(b). Combining (1) and (2) with the expression $H_{\text{eff}} = H_{\text{ms}} + H_{\text{mc}}$, the MC field corresponds to

$$H_{\text{mc}} = 4\pi M_s\left(\frac{f_{\text{NiCo}}}{\sqrt{C_2}} - N_M\right) \tag{3}$$

where f_{NiCo} is the normalized zero-field resonance frequency for the Ni_xCo_{1-x} ($0 \leq x \leq 1$) alloyed networks in Fig. 2(b). Using the as-obtained MS factor $N_M = 0.326$ from (2) for the dispersion relation for the NiFe sample, the resulting

MC field as a function of the Ni content (x) is displayed in the inset of Fig. 2(b). As expected, the H_{mc} field is negative and increases toward the observed limiting value for Co networks with perpendicular c-axis as the Ni content is reduced [6]. It is worth mentioning that the small negative anisotropy contribution observed for the Ni sample is not of the same origin as the MC contribution for the NiCo alloyed networks as it does not contain the HCP MC contribution of Co. This contribution could be originated by residual stresses due to the reduced diameter of the nanowires, as suggested in [15].

The magnetic properties of interconnected nanofiber networks can be further investigated from AMR measurements, as it provides information about changes in the resistivity as the angle between the directions of the magnetization (M) and current (I) is modified. Fig. 2(c) shows room temperature magnetoresistance curves, where the maximum resistance is reached near zero applied magnetic field for Ni-rich alloys, along both the IP and OOP directions. This behavior is consistent with high remanent magnetization states, where magnetization tends to be aligned with the nanowires axis due to the shape anisotropy. Conversely, as seen in Fig. 2(c), Co-rich alloys show a decrease of the resistance near zero field, as a result of the misalignment of the magnetization and the current paths originated by the competing MS and MC anisotropies. This is consistent with the decrease of the remanent magnetization seen in Fig. 1(a). In order to quantitatively analyze the magneto-transport properties for the distinct networks, a model has been elaborated to account for each AMR contribution due to all the nanowire orientations in the 3-D network. According to the AMR relation [13], the electrical resistivity of magnetized materials depends on the relative orientation (θ_0) between the electrical current along the nanowires (NWs) and the magnetization in the applied field direction, that is

$$\rho(\theta_0) = \rho_\perp + (\rho_{||} - \rho_\perp)\cos^2\theta_0 \tag{4}$$

where $(\pi/4) \leq \theta_0 \leq (\pi/2)$ and $0 \leq \theta_0 \leq (\pi/4)$ for the magnetization lying, respectively, in the IP and OOP directions and $\rho_{||}$ ($\rho_\perp$) is the resistivity of the CNW network in the high (low) resistance state when the local magnetization and current paths are parallel (perpendicular) to each other. By virtue of the uniform distribution of nanowire orientations in these angle ranges, resistance values at saturation ($\bar{\rho}_{ip}$ and $\bar{\rho}_{oop}$) in the IP and OOP configurations, correspond to average magnetoresistive values resulting from the contributions of all the current paths with different orientations with respect to the applied field direction. Therefore, the resistance values at saturation in the IP and OOP directions are obtained by averaging (4), that is

$$\begin{aligned}\bar{\rho}_{ip} &= \frac{1}{L}\int_{\pi/4}^{\pi/2}\rho(\theta_0)d\theta_0 \\ &= K_{ip}\rho_{||} + \left(1 - K_{ip}\right)\rho_\perp\end{aligned} \tag{5}$$

and

$$\begin{aligned}\bar{\rho}_{oop} &= \frac{1}{L}\int_{0}^{\pi/4}\rho(\theta_0)d\theta_0 \\ &= K_{oop}\rho_{||} + \left(1 - K_{oop}\right)\rho_\perp.\end{aligned} \tag{6}$$

In these equations, $L = \pi/4$ is the interval length of angles and $K_{ip} = (1/2) - (1/\pi)$ and $K_{oop} = (1/2) + (1/\pi)$ are constants relative to the specific topology of the interconnected fiber networks considered in this paper. Solving simultaneously the set of linear equations given by (5) and (6), along with the knowledge of the experimental $\bar{\rho}_{ip}$ and $\bar{\rho}_{oop}$ at saturation, allow to straightforwardly determine the resistance states $\rho_\perp$ and $\rho_{||}$. Then, the AMR ratio is obtained as

$$\frac{\Delta\rho}{\rho} = \frac{\rho_{||} - \rho_\perp}{\rho_{av}} \tag{7}$$

where $\rho_{av} = (1/3)\rho_{||} + (2/3)\rho_\perp$ is the average magnetoresistance in 3-D systems. The calculated $\rho_{||}$ and $\rho_\perp$ states, from (5) and (6), can be used to obtain accurate values of the AMR ratio as long as the saturated state of magnetization is reached properly. However, when the saturated state is not reached because of the presence of an additional competing anisotropy as in the case of the Co-rich networks [see Fig. 2(c)], the AMR can be obtained with good accuracy under the assumption that the $\rho_{||}$ state is known. Indeed, since this state is very close to the maximum resistance state (ρ_{max}) for most of the samples, the normalized resistance curves in Fig. 2(c) can be used to obtain accurate values of both the $\rho_\perp$ state and the AMR ratio, using either (5) or (6). The most accurate AMR values can be obtained along the IP direction because otherwise, the narrow proximity between $\bar{\rho}_{oop}$ at saturation and ρ_{max} observed in Fig. 2(c) leads to significant errors.

The validity of (7) can be verified by comparing the experimental $\bar{\rho}_{ip}$ versus $\bar{\rho}_{oop}$ variation with the theoretical expression

$$\bar{\rho}_{ip} = \frac{K_{oop}}{K_{ip}}\bar{\rho}_{oop} + \frac{K_{ip} - K_{oop}}{K_{ip}}\rho_{||} \tag{8}$$

which is obtained by combining (5) and (6). Fig. 3(a) shows the comparison between (8) and the experimental variation of $\bar{\rho}_{ip}$ versus $\bar{\rho}_{oop}$ obtained at the temperatures of 20, 150, and 290K for the entire set of alloy compositions given in percentages in the range from 0% to 100% and displayed by different symbols. As seen, (7) is clearly validated from the very good agreement between the model and the most of the experimental data for whatever temperature value. The strong MC anisotropy present in HCP Co-rich alloy systems is responsible for the observed deviations of $\bar{\rho}_{ip}$ versus $\bar{\rho}_{oop}$ from the model, as it prevents those systems from reaching the highest resistance state as highlighted by the decrease of the squareness of the normalized hysteresis curves shown in Fig. 2(a). Furthermore, since the application of a magnetic field in the OOP or IP direction decreases the resistance due to the AMR effect, the presence of a strong MC contribution prevents from reaching the saturated state where the complete alignment between the M and I vectors is expected. Fig. 2(a) also provides a useful guideline for the good choice of the samples that can provide accurate values of the AMR ratio. In summary, (7) is valid as long as other magnetic anisotropy contributions remain low in order to allow the resistivity from reaching the parallel ($\rho_{||}$) resistance state.

As shown in Fig. 3(b), the variation of the AMR ratio versus the Ni content (x) has been obtained from the

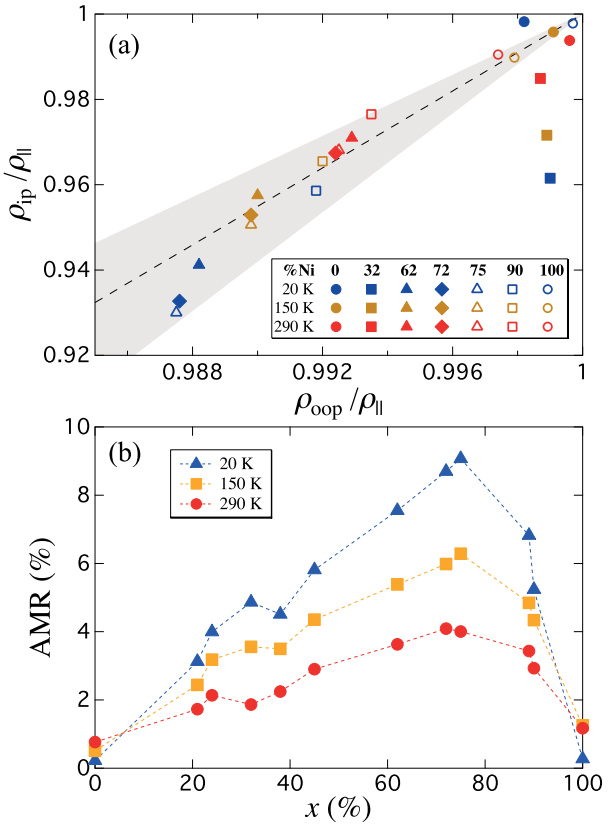

Fig. 3. (a) Comparison between the model (8) and the experimental variation of $\bar{\rho}_{ip}/\rho_{||}$ versus $\bar{\rho}_{oop}/\rho_{||}$ at $H = 10$ kOe for Ni_xCo_{1-x} interconnected fiber networks at the three temperatures of 20, 150, and 290K. The gray shaded area represents the calculated $\bar{\rho}_{ip}/\rho_{||}$ in the angle range $40° - 50°$. (b) Variation of the AMR ratio with respect to the Ni content at 20 K, 150 K, and 290 K [7].

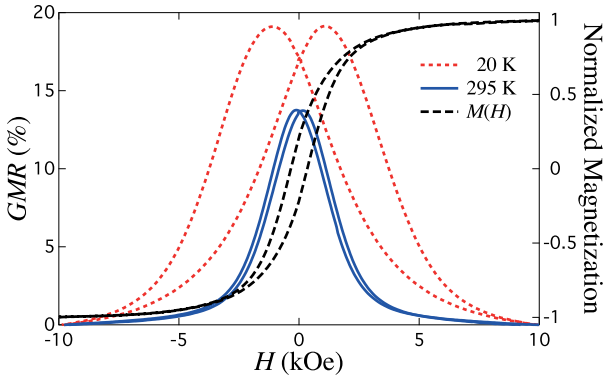

Fig. 4. Comparison of the CPP-GMR and hysteresis loop of crossed Co(10 nm)/Cu(10 nm) NWs at room temperature by applying the external field in the IP direction. The GMR curve obtained at 20 K for the same sample is also shown.

measured IP resistance at saturation ($\bar{\rho}_{ip}$) as input parameter into (7), at 20, 150, and 290K for the different Ni_xCo_{1-x} systems. As seen, the maximum AMR ratio at $x \approx 75\%$ for all temperatures is consistent with previous reports on electrodeposited CNWs, films, and metallurgically processed NiCo alloys [7], [11]–[13]. Although the AMR ratio in the interconnected nanofiber network structures increases at low temperature as a result of the smaller resistivity of the alloys, it remains slightly smaller in comparison with bulk materials as a consequence of the larger residual resistivity due to scattering by static lattice defects and surface roughness. However, the still fairly large AMR ratio obtained around 75% atomic of Ni makes this system very attractive to explore other magnetic effects as the presence of domain walls at the crossing zones, which is of particular interest for the development of AMR sensors.

On the other hand, interconnected Co/Cu multilayered 3-D nanofiber networks (40 nm in diameter) display large current perpendicular to the plane (CPP)—giant magnetoresistance (GMR) responses measured with the current flowing perpendicularly to the plane of the layers in the individual nanowire segments and thus overall in the plane of the 3-D network film.

The measurements were conducted at 290 and 20K with the applied magnetic field along the IP direction. Fig. 4 shows the CPP-GMR curves obtained at the two distinct temperatures. The GMR ratio, defined as $[\rho(H) - \rho(H_{sat})]/\rho(H_{sat})$ with H_{sat} the saturation field and expressed as a percentage, reach 14% at 295K and 19% at 20K. The magnetization hysteresis loop for the same multilayered NW sample measured in the IP direction at 295K is also shown in Fig. 4 for comparison. The GMR ratio obtained for such 3-D networks composed of Co(10 nm)/Cu(10 nm) NWs is close to the values previously reported in electrodeposited Co/Cu NWs organized in parallel arrays using nanoporous templates with similar pore diameters in the range $30 - 40$ nm [14], [16]–[19]. From previous works, it is known that the relatively large Cu layer thickness of 10 nm does not give rise to any significant antiferromagnetic exchange coupling between the layers [19]. Therefore, the magnetic layers are in the uncoupled regime, and in this case, the magnetizations in the ferromagnetic layers are randomly aligned in zero magnetic field. When the magnetic field is increased, the magnetic moments of each Co layer align in the field direction, thus leading to a decrease in the resistance.

Finally, other 3-D nanofiber network architectures based on nanotubes and core-shell nanocables are currently investigated. A wide range of controllable parameters that can be used to tune the magnetic and magneto-transport properties of mechanically stable and self-supported 3-D interconnected nanofiber networks. Numerical simulations are in progress to provide a better understanding of the studied systems. These mechanically stable 3-D nanofiber superstructures have potential applications in many fields.

IV. Conclusion

In this paper, a series of alloyed NiCo interconnected nanofiber networks has been fabricated with controlled composition by controlling the deposition potential and using different electrolytic solutions. The ease of carrying out magneto-transport measurements in these alloyed interconnected networks and the interplay between the tunable magnetic and magneto-transport properties, as a key feature for the accurate determination of magneto-transport properties like the

AMR ratio, has been demonstrated. Besides, among the advantages of the interconnected nanowire architecture are their mechanically stable and self-supporting features after chemical dissolution of the polymer membrane. The AMR ratio of these interconnected nanofiber networks has been precisely determined from simple magneto-transport measurements by proposing a simple analytical model based on the particular interconnected topology of the networks. The feasibility to obtain giant magnetoresistive responses in Co/Cu multilayered CNW networks made them very interesting structures for potential applications of 3-D nanowire networks in magnetic memory, sensor, and logic devices. Finally, this paper opens up the possibility for a controlled synthesis of complex nanoarchitectures with tunable magnetic and magneto-transport properties.

ACKNOWLEDGMENT

The authors would like to thank Dr. E. Ferain and the it4ip Company for supplying polycarbonate membranes and for providing help in obtaining SEM images. This work was supported in part by Fédération Wallonie-Brussels, Supracryst, under Grant ARC 13/18-052 and in part by the Fonds de la Recherche Scientifique—FNRS under Grant n T.0006.16. The work of J. De La Torre Medina was supported in part by CONACYT and in part by the 2017 UNAM-DGAPA-PAPIIT under Projects CB-177896 and IA101617. The work of T. da Câmara Santa Clara Gomes was supported by the National Fund for Scientific Research (FNRS).

REFERENCES

[1] E. J. W. Crossland *et al.*, "A bicontinuous double gyroid hybrid solar cell," *Nano Lett.*, vol. 9, no. 8, pp. 2807–2812, Aug. 2009.

[2] W. Wang, M. Tian, A. Abdulagatov, S. M. George, Y.-C. Lee, and R. Yang, "Three-dimensional Ni/TiO_2 nanowire network for high areal capacity lithium ion microbattery applications," *Nano Lett.*, vol. 12, no. 2, pp. 655–660, Feb. 2012.

[3] O. S. Kwon, S. J. Park, H. Yoon, and J. Jang, "Highly sensitive and selective chemiresistive sensors based on multidimensional polypyrrole nanotubes," *Chem. Commun.*, vol. 48, no. 85, pp. 10526–10528, Oct. 2012.

[4] E. Araujo *et al.*, "Artificially modified magnetic anisotropy in interconnected nanowire networks," *Nanoscale*, vol. 7, no. 4, pp. 1485–1490, Jan. 2015.

[5] G. Hrkac, J. Dean, and D. A. Allwood, "Nanowire spintronics for storage class memories and logic," *Philos. Trans. A, Math. Phys. Eng. Sci.*, vol. 369, no. 1948, pp. 3214–3228, Aug. 2011.

[6] T. da Câmara Santa Clara Gomes *et al.*, "Interplay between the magnetic and magneto-transport properties of 3D interconnected nanowire networks," *J. Appl. Phys.*, vol. 120, no. 4, Jul. 2016, Art. no. 043904.

[7] T. da Câmara Santa Clara Gomes, J. De La Torre Medina, M. Lemaitre, and L. Piraux, "Magnetic and magnetoresistive properties of 3D interconnected NiCo nanowire networks," *Nanosc. Res. Lett.*, vol. 11, Oct. 2016, Art. no. 466.

[8] M. Darques, A. Encinas, L. Vila, and L. Piraux, "Controlled changes in the microstructure and magnetic anisotropy in arrays of electrodeposited Co nanowires induced by the solution pH," *J. Phys. D, Appl. Phys.*, vol. 37, no. 10, pp. 1411–1416, Apr. 2004.

[9] A. Fert and L. Piraux, "Magnetic nanowires," *J. Magn. Magn. Mater.*, vol. 200, nos. 1–3, pp. 338–358, Oct. 1999.

[10] J. De La Torre Medina, M. Darques, A. Encinas, and L. Piraux, "Dipolar interactions in multilayered $Co_{0.96}Cu_{0.04}$/Cu nanowire arrays," *Phys. Statist. Soli*, vol. 205, no. 8, pp. 1813–1816, May 2008.

[11] N. Myung and K. Nobe, "Electrodeposited iron group thin-film alloys: Structure-property relationships," *J. Electrochem. Soc.*, vol. 148, no. 3, pp. C136–C144, Mar. 2001.

[12] B. G. Tóth, L. Péter, Á. Révész, J. Pádár, and I. Bakonyi, "Temperature dependence of the electrical resistivity and the anisotropic magnetoresistance (AMR) of electrodeposited Ni-Co alloys," *Eur. Phys. J. B*, vol. 75, no. 2, pp. 167–177, May 2010.

[13] T. McGuire and R. Potter, "Anisotropic magnetoresistance in ferromagnetic 3D alloys," *IEEE Trans. Magn.*, vol. 11, no. 4, pp. 1018–1038, Jul. 1975.

[14] L. Piraux *et al.*, "Giant magnetoresistance in magnetic multilayered nanowires," *Appl. Phys. Lett.*, vol. 65, no. 19, pp. 2484–2486, Jul. 1994.

[15] J. De La Torre Medina *et al.*, "Large magnetic anisotropy enhancement in size controlled Ni nanowires electrodeposited into nanoporous alumina templates," *Nanotech.*, vol. 27, no. 14, Feb. 2016, Art. no. 145702.

[16] K. Liu, K. Nagodawithana, P. C. Searson, and C. L. Chien, "Perpendicular giant magnetoresistance of multilayered Co/Cu nanowires," *Phys. Rev. B, Condens. Matter*, vol. 51, no. 11, pp. 7381–7384, Mar. 1995.

[17] T. Ohgai, X. Hoffer, A. Fabián, L. Gravier, and J.-P. Ansermet, "Electrochemical synthesis and magnetoresistance properties of Ni, Co and Co/Cu nanowires in a nanoporous anodic oxide layer on metallic aluminium," *J. Mater. Chem.*, vol. 13, no. 10, pp. 2530–2534, Sep. 2003.

[18] X.-T. Tang, G.-C. Wang, and M. Shima, "Perpendicular giant magnetoresistance of electrodeposited Co/Cu-multilayered nanowires in porous alumina templates," *J. Appl. Phys.*, vol. 99, no. 3, Feb. 2006, Art. no. 033906.

[19] B. Voegeli, A. Blondel, B. Doudin, and J. P. Ansermet, "Electron transport in multilayered Co/Cu nanowires," *J. Magn. Magn. Mater.*, vol. 151, no. 3, pp. 388–395, 1995.